# Modeling, Simulation, and Validation of Magneto-Rheological Dampers with LabVIEW


Adrian Olaru
Machine and Manufacturing Sys. Dept.
University Politehnica of Bucharest
Bucharest, Romania
aolaru_51@ymail.com

Ellips Masehian
Industrial and Mfg. Dept.
Cal Poly Pomona
California, USA
masehian@cpp.edu

Serban Olaru
Mechatronics Dept.
ACTTM Agency
Bucharest, Romania
serban1978@yahoo.com

Niculae Mihai
General Manager
Technoaccord Company
Quebec, Canada
mniculae@gmail.com



***Abstract*— A well-known method for optimization of dynamic behavior of industrial robots is through applying magneto-rheological dampers in robots joints. In this paper, a new mathematical (virtual) model of a magneto-rheological damper for optimizing the dynamic behavior of robots is proposed which closely simulates a real damper, as validated by experimental research. The investigated dynamic behavior parameters include viscose global dynamic damper coefficient (VGDDC), viscose global dynamic damper equivalent coefficient (VGDDEC), global dynamic transmissibility (GDT), and global dynamic compliance (GDC). The effect of these parameters on the magneto-rheological damper is analyzed on an arm-type robot and compared to no magneto-rheological damping situation. The experimental setting of the damping force versus the intensity of the magnetic field and methods to optimize the dynamic behavior are also shown. The mathematical matrix-vector model for dynamic behavior analysis of the IR is presented with the viscous friction force, depending on the intensity of the applied electrical field, the force determining the online control of the variation of torque, and the Fourier vibration spectrum. Through new multi-parameter equations, the pattern adjustment operation to the real model becomes very simple and accurate.**



***Keywords*—** Magneto-Rheological Damper; mathematical modeling; Dynamic behavior parameters; LabVIEW instrumentation.


## I. INTRODUCTION

Magneto-rheological (MR) suspensions are particle systems that under the effect of magnetic fields can increase their viscosity by two to six orders of magnitude, going from liquid state to solid state at millisecond intervals [1-3]. When applying a magnetic field, MR materials have the ability to change their viscosity by up to six orders of magnitude due to the formation of aligned particle chains. The phenomenon is illustrated in Fig. 1. The formation of "pearl chains", as aligned particle strings are called (Fig. 1(b)), is accompanied by changes in rheological (elasticity, plasticity, viscosity), as well as magnetic, electrical, thermal, and acoustic properties, although the major effect is the increase in apparent viscosity. When removing the magnetic field, the particles return to the disordered state of Fig. 1(a) [4-5]. MR materials are composed of three major components: *ferromagnetic particles* (20−50%) such as FeCO, *carrier fluid* like water, glycol, kerosene and synthetic or mineral oil (silicone), and stabilizer for keeping the particles suspended in the fluid, such as silica gel.

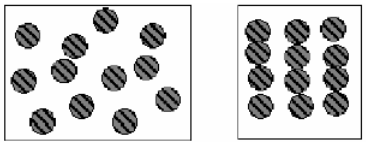

**Fig. 1.** Schematic illustration of the reversible particle behavior of MR materials: (a) disordered layout in the absence of external magnetic field; (b) alignment in a single direction field application [4].

A 'good' MR material is characterized by low initial viscosity, high shear stress values at certain magnetic field strengths, negligible temperature dependence, and high stability. Regarding the influence of the intensity of the applied magnetic field on the voltage variation with the shear rate, the shear stress stabilizes with increasing shear rate but increases proportional to the square root of the intensity of the applied magnetic field [4].

### *A. Magneto-Rheological Damper Models*

Magneto-Rheological Dampers (MRD) are shock absorbers that are filled with magnetorheological fluid and can be controlled by changing the power (intensity) of an electromagnet: by increasing the power, the fluid viscosity also increases, and thus the damper's shock absorbing characteristics are controlled. In order to simulate its actual behavior, various researchers have attempted to mathematically model MRDs, proposing parametric or nonparametric models. The comparison between theoretical models and the real behavior is possible through experimental assisted plotting of some characteristics of the damper [5-9].

The Bouc-Wen model is more extensive and complex, includes the hysteresis curve, and requires a closed loop control algorithm [10-12]. In the MR model proposed in [13] the magnetorheological material operates in two rheological domains: precursor and passage, and the modeling is done using constant coefficients of viscous damping and generalized forces with linear evolution, and inconsistent. The Choi model [7, 14] proposes a sixth polynomial model that does not consider hysteresis. Gamota and Filisko [15] represent an extension of the Bingham model describing electro-rheological (ER) behavior in the pre-flow and post-flow states. The model highlights the presence of hysteresis, but is not accurate enough compared to real behavior since it uses constant coefficients that control precisely the areas in the damping force characteristic.

The three-piece Powell model proposed in [16, 17] does not sufficiently consider hysteresis, which is numerically controlled only by the introduced static and dynamic coefficients. The BingMax model with discrete elements presented in [18, 19] is too complicated to transpose into a numerical simulation model, and the nonlinear visco-elastic-plastic model presented in [20, 21] combines two linear flow mechanisms with nonlinear functions: both models are excessively theoretical, without being close to real state, as seen by comparing characteristics. The bi-viscous model [22, 23] is linearized by introducing two slopes for elastic and viscous functioning but does not address hysteresis. Non-parametric MRD models are based performance and usually require acquisition of experimental data on the behavior of different tasks under different conditions. Models proposed in this category are based on Chebychev polynomials [24, 25], neural networks, or the identification techniques. A few works by the authors also exist on numerical simulation of dynamic parameters of single or multiple robots and their drives, dampers, etc. using the LabVIEW instrumentation [26-31].

Analysis of the existing literature shows a research gap in MRD modeling approaches that through numerical simulations clearly indicate the differences between real and theoretical MRD models and facilitate compensating for inappropriate instances. Therefore, in this paper, we present a numerical simulation and data acquisition for MRD with the help of the LabVIEW instrumentation and show its precision in simulating a real MRD.

## II. The Proposed Mathematical Model for Magneto-Rheological Damper

Most of the damper models developed by various researchers either do not take into account the hysteresis phenomenon present in real behavior (as in Bingham's model), or approximate the values and aliases of real model characteristics with a large error (as in Parker and Powell's model). The closest model we could find for simulation of the real MRD is the Bouc-Wen model [10-12] (Fig. 2), which we adopted in this research. However, the Bouc-Wen model has some differences with real dampers in the hysteresis zone, in the beginning and end zones of the damping force action, as well as on the slopes in both compression and extension zones. Therefore, in order to closely replicate a real MR damper and minimize the Bouc-Wen models' errors, we improved it by adding new equations and several parameters. Furthermore, in the original Bouc-Wen model, the hysteresis curve is not consistent over the frequency spectrum and peak frequencies are variable. In our proposed modified model, however, a frequency-dependent hysteresis coefficient is introduced that is expressed by a periodic function as the sum of sinusoids.

By adjusting the newly introduced 19 parameters (including Viscose Global Dynamic Damping Coefficient (VGDDC), the Viscose Global Dynamic Damping Equivalent Coefficient (VGDDEC), the Local Dynamic Compliance (LDC), and Global Dynamic Compliance (GDC)), we are able to minimize the inconsistency and errors between the model and the real damper to less than 1%, as suggested by the results of extensive simulations of the damper on LabVIEW. Using the LabVIEW enabled us to adjust the coefficients of the improved mathematical model and analyze the influence of the coefficients on the dynamic behavior and hence the damping force vs. speed of motion characteristic. The mathematical matrix model of the active torque and damping force are presented in eq. (1), eq. (2), and Table 1.

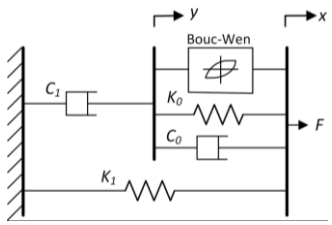


**Fig. 2.** Schematic illustration of the Bouc-Wen damper's model.

$$
\begin{aligned}
&f = c_0(x'-y') + k_0(x-y) + k_1(x-x_0) + \alpha z \\
&y' = \frac{1}{c_0+c_1}[\alpha z + c_0 x' + k_0(x-y)] \\
&z' = -\gamma|x'-y'|z|z|^{n-1} - \beta(x'-y')|z|^n + \delta(x'-y') \\
&\delta = \sum \delta_{0i}\sin(2\pi\upsilon_i + \phi_i) \\
&\alpha(i) = \alpha_3 i^3 + \alpha_2 i^2 + \alpha_1 i + \alpha_0 \\
&c_0(i) = c_{03} i^3 + c_{02} i^2 + c_{01} i + c_{00} \\
&c_1(i) = c_{13} i^3 + c_{12} i^2 + c_{11} i + c_{10} \\
&k_0(i) = k_{03} i^3 + k_{02} i^2 + k_{01} i + k_{00}
\end{aligned}
\tag{1}
$$

Table 1. Definitions of the proposed MRD model's parameters and variables.

| Parameter/Variable and its Description | | Unit |
|---|---|---|
| $F$ | active force matrix in the robot's joints | N |
| $M$ | active moment matrix | Nm |
| $F_R$ | resistive force matrix reduced in the robot's gravity center | N |
| $M_R$ | resistive moment matrix reduced in the gravity center | Nm |
| $D_i^{i-1}$ | transfer matrix from $i$ to $i$–1 Cartesian system | – |
| $G_i$ | body-joints matrix | – |
| $Z_u$ | joints-bodies matrix | – |
| $m_u$ | diagonal matrix of robot mass | – |
| $J_i$ | matrix form of the inertial tensor | Nms$^2$/rad |
| $a^i_{i,0}$ | acceleration matrix of the gravity center | m/s$^2$ |
| $r^i_{gi}$ | position vector | m |
| $\omega^i_{i-1,0}$ | asymmetrical matrix of the angular velocity vector | rad/s |
| $\varepsilon^i_{i,\,i-1}$ | matrix form of the relative angular acceleration | rad/s$^2$ |
| $f(i)$ | damping force | N |
| $x$, $y$ | primary and secondary displacement variables | m |
| $z$ | internal history dependency variable of the MRD | m |
| $k_0$, $k_1$ | nonlinear internal rigidity of the MRD [N/m] depending on the current intensity $i$ | A |
| $c_0$, $c_1$ | internal viscous damping parameters of the MRD | Ns/m |
| $x_0$ | perturbation displacement | m |
| $\alpha$ | internal parameter that has nonlinear evolution and depends on the magnetic variable field (electrical intensity) | – |
| $\beta$ | parameter characterizing the gain of increasing of the damping force versus velocity | – |
| $\delta$ | hysteresis parameter | – |

$$
\begin{pmatrix} F \\ M \end{pmatrix} = \begin{bmatrix} z_u & \mathbf{0} \\ \mathbf{0} & z_u \end{bmatrix} \begin{pmatrix} D_{0,i}(F_R^i + f(i)) \\ D_{0,i} M_R^i \end{pmatrix} - diag\left[ sign\frac{v_u^i}{|v_u^i|} m_{u_i} \quad sign\frac{\omega_u^i}{|\omega_u^i|} J_{g_i} \right] \cdot \begin{pmatrix} \left(a_{i,0}^i\right) + \left[\tilde{\omega}_{i,0}^i\right]^2 \left(r_{g_i}^i\right) \\ \left(\varepsilon_{i,i-1}^i\right) + \left[\omega_{i-1,0}^i\right]\left(\omega_{i,i-1}^i\right) \end{pmatrix} + \begin{bmatrix} z_u & \mathbf{0} \\ \mathbf{0} & z_u \end{bmatrix} \cdot \left[ \begin{matrix} \mathbf{0} \\ \left[G_{i,k}\right]\left(\tilde{b}_{i,k}\right)\left( \left(D_{0,i}\left(F_R^i + f(i)\right)\right) - diag\left[ sign\frac{v_u^i}{|v_u^i|} m_{u_i} \right] \cdot \left[D_{0,i}\right]\left( \left(a_{i,0}^i\right) + \left[\tilde{\omega}_{i,0}^i\right]^2 \left(r_{g_i}^i\right) \right) \right) \end{matrix} \right] \tag{2}
$$

## III. EXPERIMENTAL RESEARCH USING LABVIEW

A number of parameters of the MRD model are introduced to describe different regions of the damping force vs. speed curve (Fig. 3), as follows: $p_1$ – the slope of the characteristic in the expansion phase; $p_2$ – the slope of the feature in the compression phase; $p_3$ – the slope of the characteristic at the top of the hysteresis curve; $p_4$ – maximum hysteresis at minimum speed; $p_5$ – the size of hysteresis at maximum speed; $p_6$ – ordered by the quasi-linear feature; $p_7$ – maximum order of the feature; $p_8$ – maximum feature on the abscissa; and $p_9$ – the abscissa of the hysteresis peak. By altering the values of all coefficients and comparing traits of the characteristics, it will be possible to determine how the various parameters are affected by the changes of the coefficients of the mathematical model. Also, it is possible to adjust the force characteristics versus velocity so that the form of the characteristic approaches the experimentally determined value.

Fig. 4 shows some snapshots of the numerical simulation of the MRD using the LabVIEW software. By analyzing the output, the following conclusions can be made: changing the intensity of the electric current affects the parameters $p_1$, $p_2$, $p_6$, and $p_7$; changing the displacement perturbation $x_a$ affects the parameters $p_3$ and $p_5$; changing the internal coefficient $\gamma$ affects the parameters $p_3$ and $p_5$; changing the vibration amplitude $x$ affects the parameters $p_7$, $p_8$, and $p_9$; changing the global stiffness $k_1$ affects the parameters $p_3$, $p_4$, $p_5$ and $p_7$; changing the damping force amplification $\beta$ affects the parameters $p_3$, $p_6$, and $p_7$; modification of the term hysteresis $\delta$ affects the parameters $p_1$, $p_2$, $p_3$, $p_4$, $p_5$, and $p_9$; modifying the internal order of $\alpha_2$ affects the parameters $p_3$, $p_6$, and $p_7$; modifying the internal coefficient of the order $\alpha_1$ affects the parameters $p_3$, $p_6$, $p_7$, and $p_9$; and finally, the modification of the second-order viscosity damping coefficient $c_{02}$ causes the parameter $p_3$ to change.

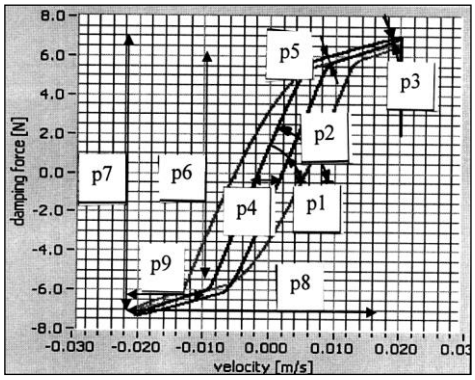


**Fig. 3.** Parameterized damper force characteristic versus velocity.

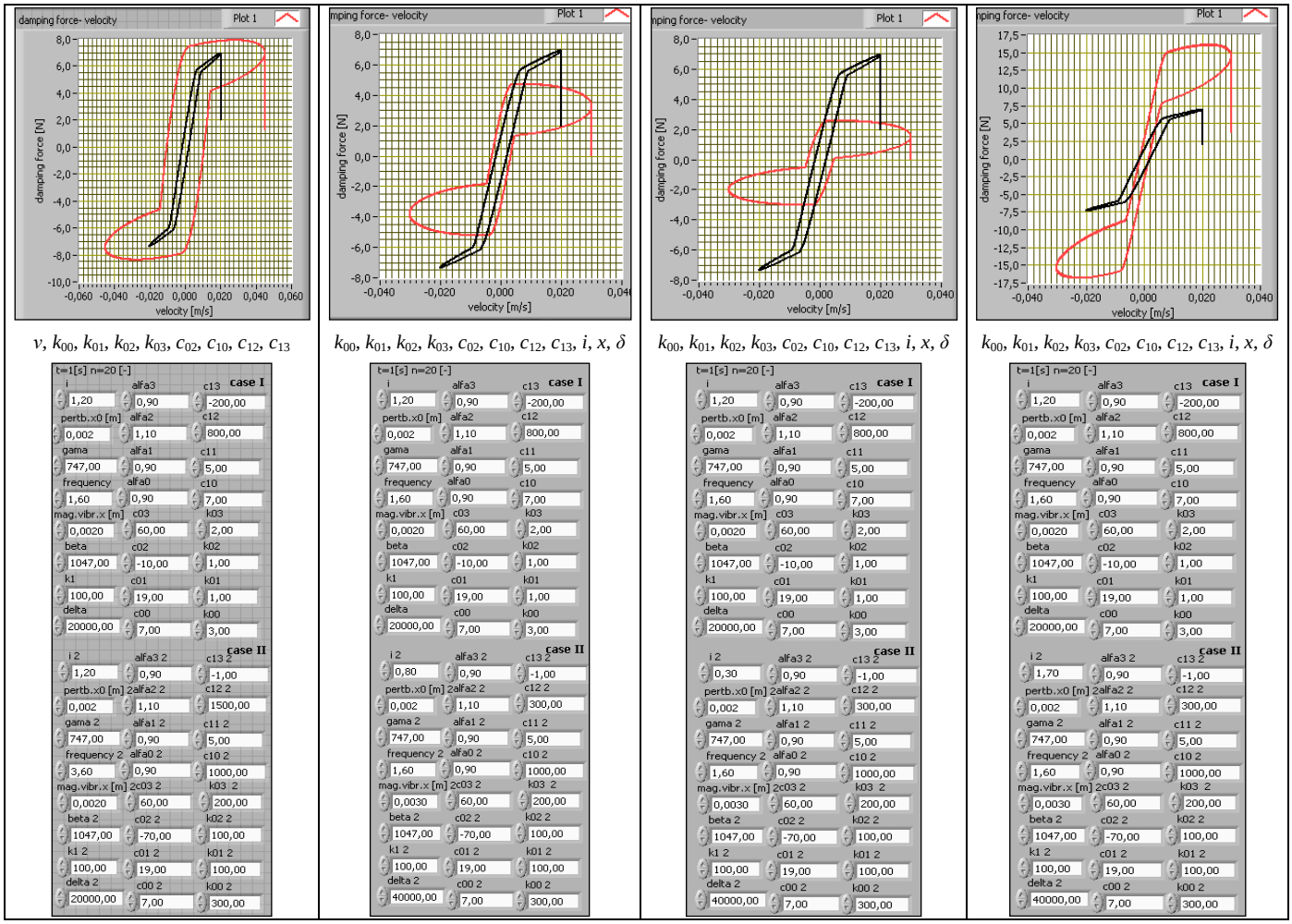


**Fig. 4.** Snapshots of LabVIEW simulation of the MRD characteristic damper force vs. velocity.

The implementation of magneto rheological dampers in the structure of robots was performed to reduce the vibrations with certain frequencies and amplitudes, by which the instability of the movement can be determined. Indeed, our experimental results showed that these vibrations are either attenuated or transferred to a higher frequency range.

Our experimental setup for testing the developed MRD includes the following components:

- A U-shaped articulated didactic robot developed in the Dynamic Behavior Research Lab at Politehnica University of Bucharest,
- Electro-dynamic excitation (type RFT 11075),
- LP connector type CB-68,
- Acquisition board PCI 6221 M,
- Frequency generator type POF-1, KABID,
- Amplifier for frequency generator type LV 102, MMF, inductive displacement transducer type 16.1 IAUC,
- bridge; type KWS/T-5,
- Magneto-rheological damper,
- Desktop PC with LabVIEW software version 8.2.

The LabVIEW virtual instrumentation is a specialized tool for fast and low-cost research on dynamic behaviors of electromechanical components. The assisted experiments research was performed based on the developed MRD mathematical model using the LabVIEW with the aim of obtaining some specific features such as force vs. speed, force vs. displacement, damping force and displacement speed vs. time, and damping energy vs. time.

The experiments consisted of excitement at the base of the robot's structure with a periodic force of variable frequency and simultaneous determination of five acquisition channels reading the excitation force, damping force, end-effector displacement, acceleration at base, and acceleration at end-effector. Figs. 5-9 show the LabVIEW panels for experimental analysis, whereas Fig. 10 shows its panel for theoretical research. The virtual instrument for assisted data acquisition includes several modules: the input digital motion control data, task/ channels in - MyDigitalOut Task0, command line, lines -dev 1 /port0 /line0, where dev1 is the used acquisition board PCI 6224M, port0line0, is the port and the digital control line, the mode of entering task/channels acquisition data, DAQ Assistant 20, the mode for entering active port data, centesimal, stop motion control button, mediated data acquisition mode, linear-type average, etc. The electric connections for acquiring acceleration on the robot's base are shown in Fig. 11.

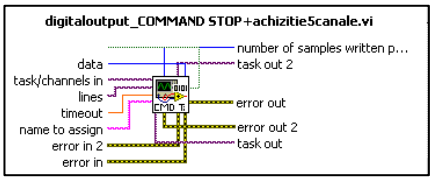


**Fig. 5.** LabVIEW icon for data acquisition.

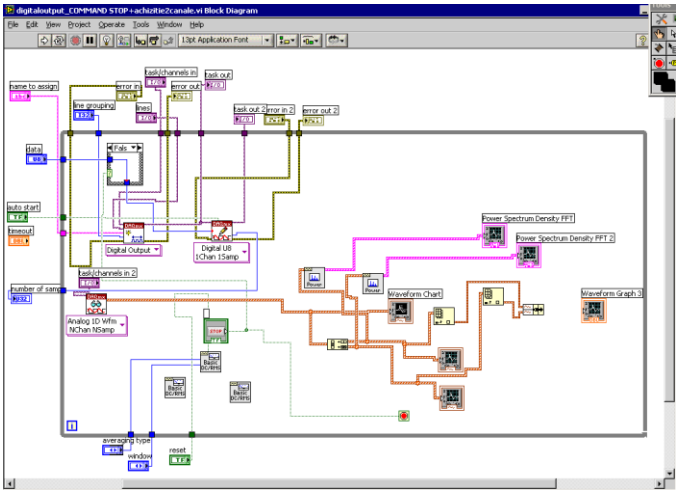

**Fig. 6.** The block schema of the LabVIEW virtual instrument.

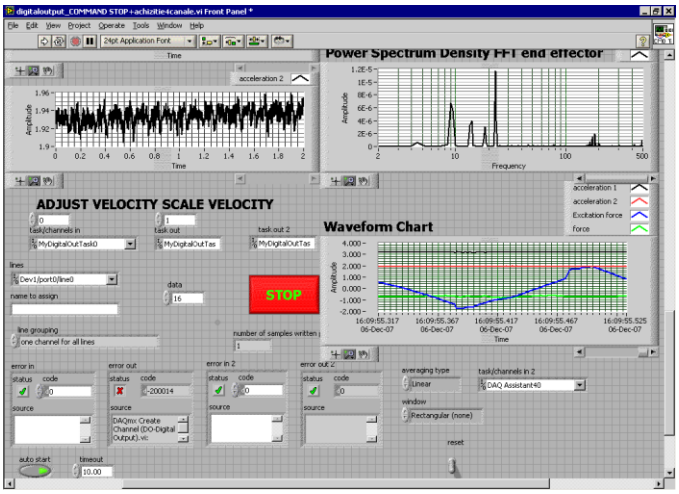


**Fig. 7.** Front panel with the results of acquisition with 6 channels.

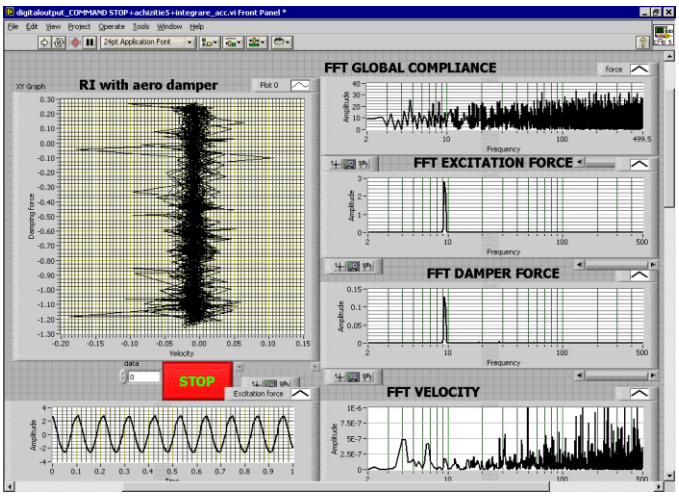


**Fig. 8.** Front panel of the LabVIEW virtual instrument for the acquisition

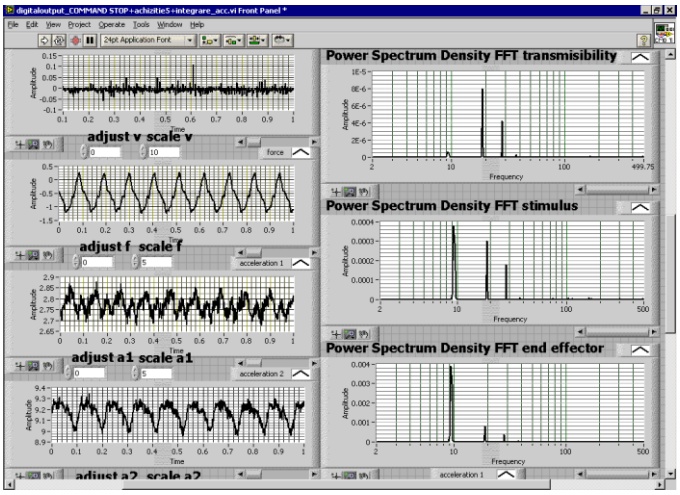


**Fig. 9.** Front panel with real and simulated frequency characteristics.

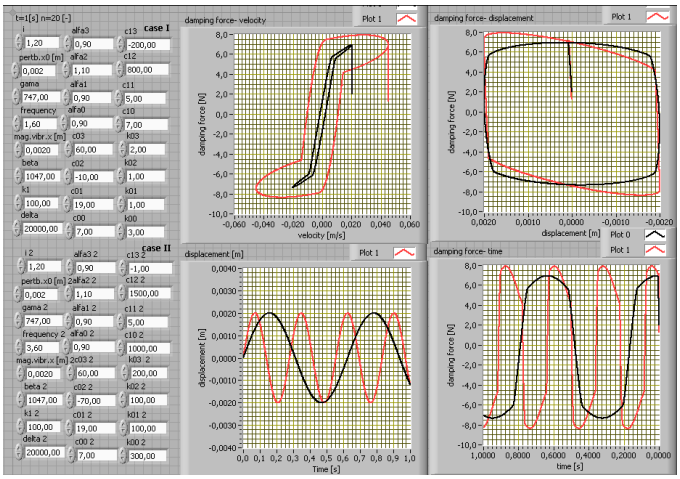


**Fig. 10.** Virtual LabVIEW instrument for the theoretical assisted research.

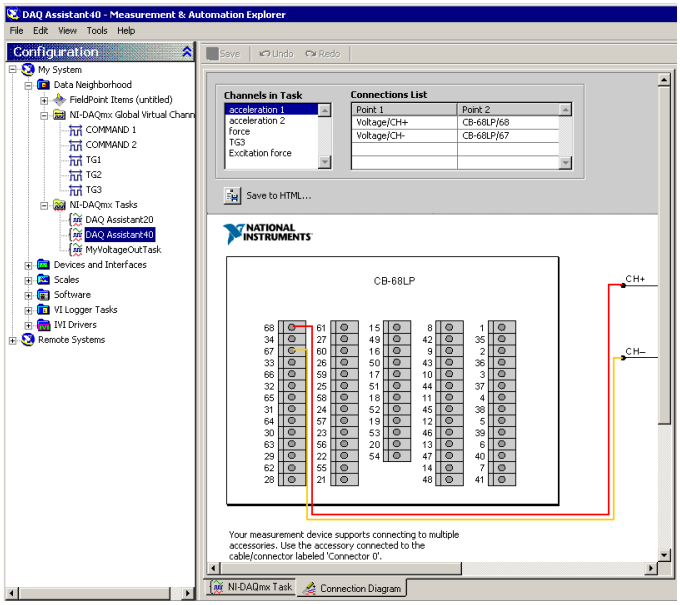


**Fig. 11.** Electrical connections for acquiring acceleration at the robot's base.

Validation of the proposed mathematical model was performed by experimental determination of force vs. velocity characteristics and their comparison with the characteristics determined by numerical simulation. In the first phase, the comparison was done between the experimentally obtained characteristics and those generated by the modified Bouc-Wen mathematical model [10-12]. It was observed that these characteristics were very different, which led us to the work out a more elaborate mathematical model supplemented with four additional equations and another equation to takes into account the Fourier spectrum. In this case, the proposed mathematical model has 19 new parameters to facilitate the identification process. The mathematical model for the MRD used in the experimental research and validated by the comparative method is presented as follows:

$$
\begin{aligned}
f &= c_0(x'-y') + k_0(0.003-y) + 100(x-0.002) + \alpha z \\
y' &= \frac{1}{c_0+c_1}[\alpha z + c_0 x' + k_0(0.003-y)] \\
z' &= -747|x'-y'|z|z|^{n-1} - 1047(x'-y')|z|^n + 40000(x'-y') \\
\alpha(i) &= 0.9i^3 + 1.1i^2 + 0.9i + 0.9 \\
c_0(i) &= 60i^3 - 70i^2 + 19i + 7 \\
c_1(i) &= -i^3 + 300i^2 + 5i + 1000 \\
k_0(i) &= 200i^3 + 100i^2 + 100i + 300 \\
\delta &= 50\sin(10\pi + 0.21) + 1.1\sin(18\pi + 0.31) + 1.4\sin(30\pi + 0.62)
\end{aligned}
\tag{3}
$$

By using the LabVIEW virtual instruments for simulation, it was possible to identify the coefficients, which ultimately led to attaining a comparative force vs. speed characteristic with a maximum error of less than 1% relative to the real characteristics. For the assisted determination of the coefficients of the mathematical model, it was switched to the parameterization of the force vs. velocity characteristic, so that by the numerical simulation we could determine how the various coefficients of the mathematical model influence the various parameters of the characteristic. Obviously, the precise parameter setting led to the achievement of features as close as possible to their real counterparts.

Based on extensive comparisons of the various characteristics obtained by the simulation with those obtained experimentally, we obtained the approximation presented in Fig. 12. In addition, the real force-velocity characteristics experimentally determined for the investigated didactic robot on which the air damper and magneto rheological damper MRD were mounted are presented in Fig. 13.

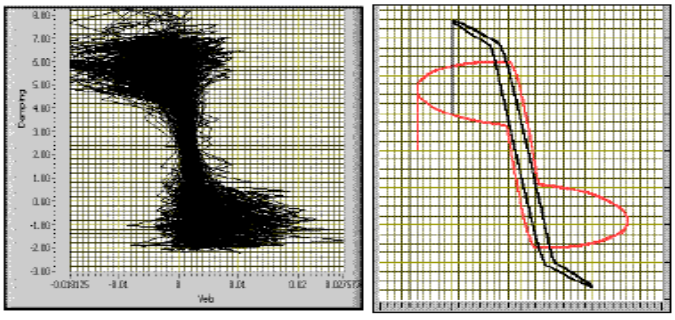

**Fig. 12.** The real and theoretic damper force vs. velocity characteristic.

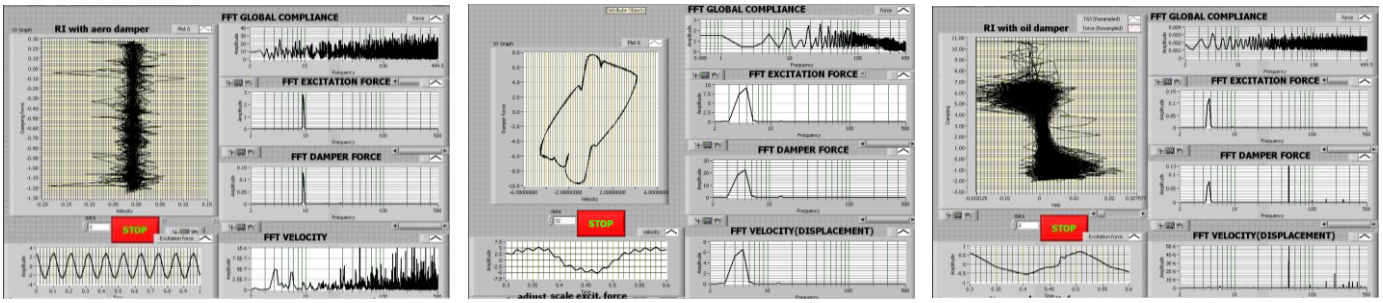


(a) Without damper 5 Hz excitation frequency (b) With air damper 5 Hz excitation frequency (c) With MRD 5Hz excitation frequency

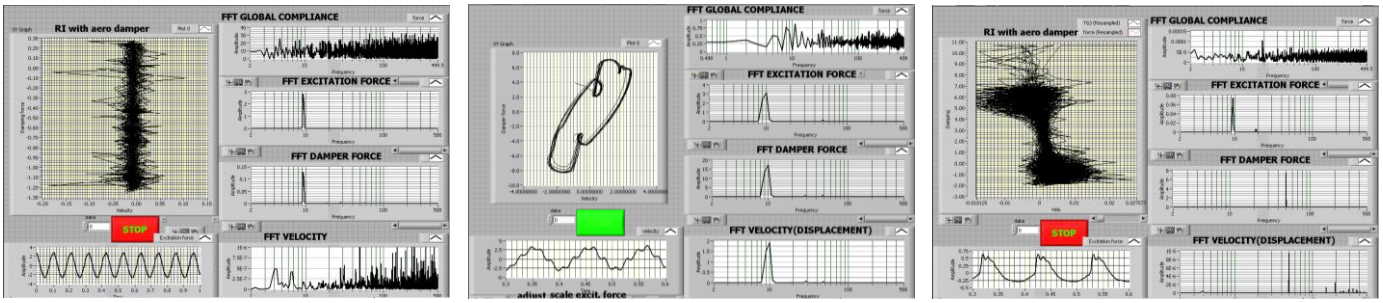


(d) Without damper 12 Hz excitation frequency (e) With air damper 12 Hz excitation frequency (f) With MRD 12 Hz excitation frequency

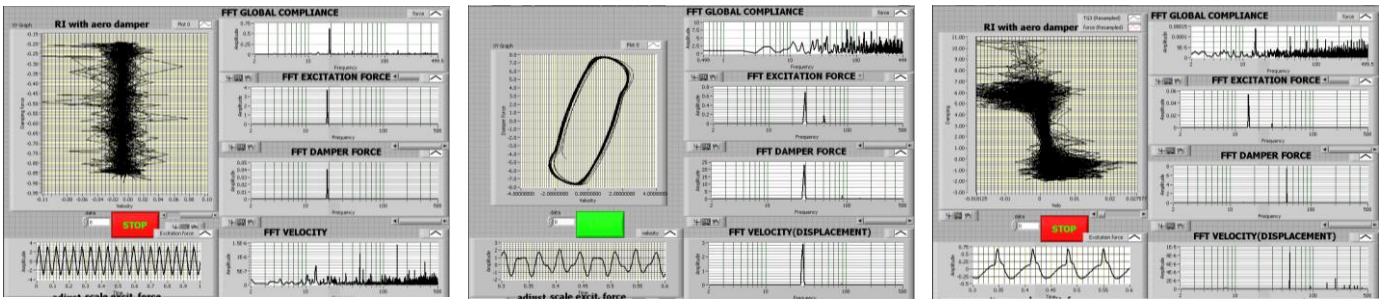


(g) Without damper 25 Hz excitation frequency (h) With air damper 25 Hz excitation frequency (i) With MRD 25 Hz excitation frequency

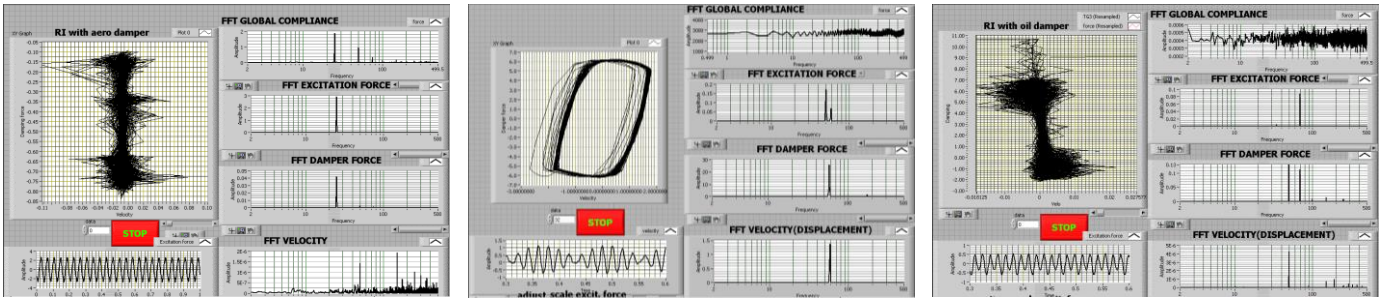


(j) Without damper 38 Hz excitation frequency (k) With air damper 38 Hz excitation frequency (l) With MRD 38 Hz excitation frequency

**Fig. 14.** Real force-velocity characteristics, experimentally determined for the robot with air and magneto rheological dampers.

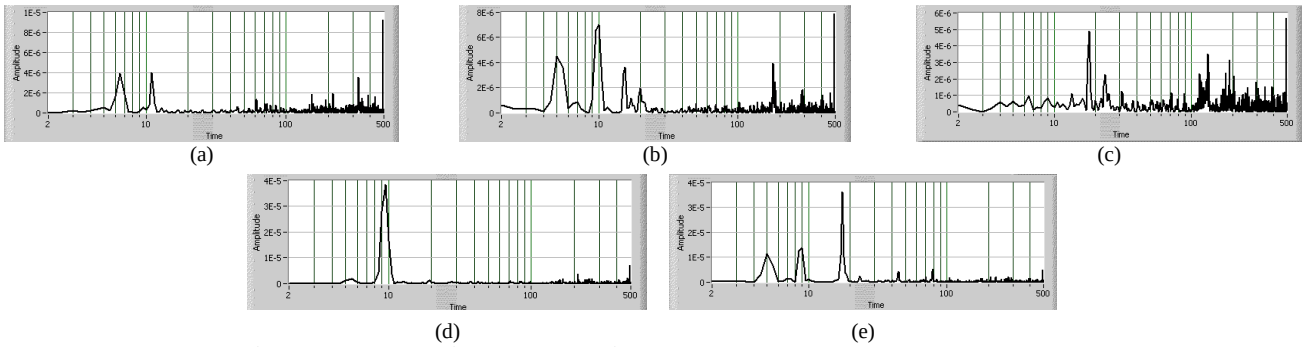


(a) (b) (c)

(d) (e)

**Fig. 15.** Fast Fourier Global Transfer Function spectrum for various cases of robot movement: (a) moving up without damper, (b) moving up with air damper, (c) moving up with MRD, (d) moving down without damper, (e) moving down with MRD.

## IV. Discussion and Analysis of Results

After analyzing the results of experimental research, the following conclusions can be highlighted:

- Utilizing dampers resulted in an increase of the first three resonant frequencies on the Fourier spectrum to higher frequencies. Specifically in the robot's upward movement, when no damper is used the peak frequencies at 1, 6, and 11 Hz (Fig. 15(a)) shifted to 5, 10, and 16 Hz when using air damper (Fig. 15(b)), and to 15, 18, and 24 Hz when using MRD (Fig. 15(c)). Likewise, in the robot's downward movement, when no damper is used the peak frequencies at 1, 5, and 9 Hz (Fig. 15(d) jumped to 5, 9, and 18 Hz when using MRD (Fig. 15(e)).
- Due to the imbalance of the robotic arm, the Fourier spectrum is different for upward and downward motions. The imbalanced weight force acts as a damper, and thus in the same damping conditions, the frequencies in upward are higher than those of the downward movement: {1, 6, 11} Hz vs. {1, 5, 9} Hz in motion without damping, and {15, 18, 24} Hz vs. {5, 9, 18} Hz in motion with magnetorheological damping.
- Transmissibility is higher in low frequencies, mostly comparable to the structure's resonant 14 Hz frequency at 10 and 20 Hz.
- The transmissibility between base and end-effector, at a 10 Hz excitation with MRD is much lower than without damping, respectively $3.5\times10^{-6}$ vs. $5.5\times10^{-6}$ at the first frequency spectrum of 10 Hz, and $2.8\times10^{-6}$ versus $4.5\times10^{-6}$ at the 20 Hz spectrum frequency.
- Transmissibility is approximately the same at excitations in higher (above 35 Hz) frequencies, which are the working frequency range of the didactic robot.
- The Global Dynamic Compliance (GDC) is higher in low excitation frequencies. For instance, for a 4 Hz frequency spectrum, it equals 20 mm/N at an excitation of 10 Hz, while it equals 0.2 mm/N for a frequency spectrum of 20 Hz and excitation of 20 Hz.
- The Global Dynamic Compliance (GDC) is maximal at an excitation of 10 Hz, which means that the robot structure has a mechanical resonance close to 10 Hz, this being at 14 Hz.
- The damping force is maximal for the air damper case at 9 Hz.
- It is possible to determine the damping energy using the analysis of the variation ratio of the damping force to the speed. The energy coefficient calculated as this ratio equals 15 (maximum value) at 10 Hz, and then it decreases to 11.66 at 25 Hz, 11.11 at 50 Hz, 10.62 at 35 Hz, 8.75 at 20 Hz, and 8.5 at 30 Hz.

## V. Conclusions and Future Work

Magneto-Rheological Dampers (MRD) are shock absorbers that are filled with magnetorheological fluid and can be controlled by changing the power (intensity) of an electromagnet. MRDs have been widely implemented in intelligent structures of industrial robots, and several theoretical models have been developed to simulate the behavior of MRDs, among which, the Bouc-Wen model is more extensive and complex, includes the hysteresis curve, and requires a closed loop control algorithm. In this paper, we have proposed an extension to the Bouc-Wen model by introducing new parameters and equations in order to remedy its weaknesses which include errors in the hysteresis zone, in the beginning and end zones of the damping force action, and in the slopes in both compression and extension zones, as well as inconsistencies of the hysteresis curve over the frequency spectrum and variability of peak frequencies.

Our proposed model was tested on a didactic manipulator using the LabVIEW virtual instrumentation by comparing the theoretical and the experimental damping force vs. speed. The theoretical research included the introduction of new parameters regarding the local and global dynamic behavior, which were tuned online using the LabVIEW for better simulating real MRDs, so that the error level was less than 1%. The dynamic behavior of the robot structure was accurately expressed by a new matrix-vector equation for determining the torque, which allows online mathematical control of the value of the forces and moments in the robot's joints. Parameterization of the damping force curves versus the linear damping speed allowed the assisted investigation to determine all (over 40) coefficients of the mathematical model on all of the specific characteristics of the dampers of this type, including damping force vs. velocity, damping force vs. displacement, damping force vs. time, displacement vs. time, and damping energy vs. time. The following dynamic parameters were determined: global dynamic compliance, transmissibility, and damping transfer function.

The results of the experimental research provide a synthetic image of the dynamic behavior of the robotic structure investigated in the variants studied, namely with a magneto rheological damper, with air damper, and without damper, with arm motions in both upward and downward directions. These results made it possible to move to the next stage, the construction and research of the dynamic behavior of a structure with intelligent schema that has the following components: an accelerometer sensor, an actuator (magneto rheological damper), software (LabVIEW for analog control), hardware (PCI 6224M acquisition board and personal computer), signal conditioners (two and three-stage amplifiers), all operated by a 12v DC power source.

The optimization included the determination of frequencies in the Fourier spectrum based on the new mathematical model of the torque, including the damping force, and its optimization by modifying the local compliance, the size of the structure, and the mass of the component bodies. We generated acceleration signals with at least 10 frequencies in the Fourier spectrum to approximate the accelerator signals acquired by the accelerometers as accurately as possible. Optimization also included the construction of the intelligent structure that enabled attenuating the vibrations from the dynamic behavior of the investigated didactic robot.

In conclusion, the proposed new model and the experimental setup can be used to facilitate the application of magneto rheological dampers in intelligent robotic structures and provides a low-error method for online control of the vibration spectrum and active torque in all joints of the robot.

Directions for future work include: (1) determination of the global dynamic coefficient of viscous damping, its representation and frequency tuning in realtime, (2) determination of the damping force by modifying the electric field, and (3) experimental determination of additional damping factors.

## REFERENCES


[1] Burton, S. A.; Makris, N.; Konstantopoulos, I.; Antsaklis, P. J.: Modeling the response of ER damper: phenomenology and emulation. Journal of Engineering Mechanics, **122** (1996), 897-906.

[2] Butz, T., Stryk, O. Modelling and Simulation of Rheological Devices, Sonderforshungsbereich 438: Tehnische Universitat Munchen, Universitat Augsburg, Preprint SFB-438-9911, 1999.

[3] Carlson, J.D., Spencer Jr., B.F. Magneto-rheological fluid dampers: scalability and design issues for application to dynamic hazard mitigation. In Proceedings of the 2nd Int. Workshop on Structural Control, Hong Kong,18-21 December 1996, 99-109.

[4] Lord Corporation: Rheonetic MagnetoRheological (MR) Fluid Technology. Cary, NC, 1997. World Wide Web: http://www.mrfluid.com.

[5] Back´e, W.; Fees, G.; Murrenhof, H.: Innovative Fluidtechnik-Hochdynamischer Servoantrieb mit elektrorheologischen Fl¨ussigkeiten. ¨Olhydraulik und Pneumatik, **41** (1997) 11/12.

[6] Böse H., Berkemeier J. and Trendler A., "Haptic System Based on Electrorheological Fluid," Proceedings of the ACTUATOR 2000 Conference, 19-21 June 2000, Bremen GERMANY.

[7] Choi S. B., "Control of ER Devices," International Journal of Modern Physics B, Vol. 13, No. 14-16, 1999, pp.2160-2167.

[8] Gavin HP., "Control of Seismically-Excited Vibration Using ER Materials and Lyapunov Methods", IEEE Transactions and Automatics Control, Vol. 9, No. 1, pp. 27-36, 2001.

[9] Jolly, M.R., Bender, J.W., Carlson, J.D., Properties and Applications of Commercial Magnetorheological Fluids.

[10] Dyke, S. J.; Spencer Jr., B. F.; Sain, M. K.; Carlson, J. D.: On the efficacy of magnetorheological dampers for seismic response reduction. 1997 ASME Design Engineering Technical Conferences, Sacramento, CA, 14-17 September 1997.

[11] Dyke, S.J., Spencer, B.F., Sain, M.K., Carlson, J.D., Application of Magnetorheological Dampers to Seismically Excited Structures, Proceedings of the 17th International Modal Analysis Conference, Kissimmee, Florida, pp. 8-11, 1999.

[12] G. Yang, B. F. Spencer, Jr., J. D. Carlson, M. K. Sain, Large-scale MR fluid dampers: modeling, and dynamic performance conside-rations, Report CMS 99-00234, 1999.

[13] Li, Y-W., Wang, J-S., Wang, L-P., Liu, X-J., "Inverse dynamics and simulation of a 3- DOF spatial parallel manipulator", Proceedings of the IEEE Int. Conf. on Robotics & Automation, Taipei, Taiwan, 2003.

[14] Choi, Y.; Sprecher, A. F.; Conrad, H.: Vibration characteristics of a composite beam containing an electrorheological fluid. Journal of Intelligent Material Systems and Structures, **1** (1990), 91-104.

[15] Gamota, D. R.; Filisko, F. E.: Dynamic mechanical studies of electrorheological materials: Moderate frequencies. Journal of Rheology, **35** (1991), 399-425.

[16] Peschel, M.J., Roschke, P.N., Neuro-Fuzzy Model of a Large Magnetorheological Damper, Proceedings Texas Section- ASCE, Spring Meeting San-Antonio, 2001.

[17] Petek, N. K.: An electronically controlled shock absorber using electrorheological fluid. Society of Automotive Engineers Technical Paper Series, Paper No. 920275, 1992.

[18] Makris, N.; Burton, S. A.; Hill, D.; Jordan, M.: Analysis and design of ER damper for seismic protection of structures. Journal of Engineering Mechanics, **122** (1996), 1003-1011.

[19] Makris, N.; Burton, S. A.; Taylor, D. P.: Electrorheological damper with annular ducts for seismic protection applications. Smart Materials and Structures, **5** (1996), 551-564.

[20] Kamath, G. M.; Wereley, N. M.: System identification of electrorheological fluid-based dampers using a nonlinear viscoelastic-plastic phenomenological model. 35th Aerospace Sciences Meeting, Reno, NV, 6-9 January 1997.

[21] Kamath, G. M.; Wereley, N. M.; Jolly, M. R.: Analysis and testing of a model-scale magnetorheological fluid helicopter lag mode damper. American Helicopt;er Society 53rd Annual Forum, Virginia Beach, 1997, 1325-1335.

[22] Stanway, R.; Sproston, J. L.; Stevens, N. G.: Nonlinear modelling of an electro-rheological vibration damper. Journal of Electrostatics, **20** (1987), 167-184.

[23] Stanway, R.; Sproston, J. L.; El-Wahed, A. K.: Applications of electro-rheological fluids in vibration control: a survey. Smart Materials and Structures, **5** (1996), 464-482.

[24] Gavin, H. P.; Hanson, R. D.; Filisko, F. E.: Electrorheological dampers, Part I: Analysis and design. Journal of Applied Mechanics, **63** (1996), 669-675.

[25] Gavin HP., "Control of Seismically-Excited Vibration Using ER Materials and Lyapunov Methods", IEEE Transactions and Automatics Control, Vol. **9**, No. 1, pp. 27-36, 2001.

[26] Olaru A., Olaru S., & Mihai N., "Proper Assisted ResearchMethod Solving of the RobotsInverse Kinematics Problem", Applied Mechanics and Materials, vol. 555, 2014, p.135-147.

[27] Olaru A., Olaru S., Ciupitu L., "Assisted research of the neural network by back propagation algorithm", OPTIROB Conference, Romania, June 2010.

[28] Olaru A., Olaru S., Mihai N. Application of a new Iterative pseudo-inverse Jacobian Neural Network Matrix technique for controlling Geckodrive DC motors of manipulators, 3rd RSI Int. Conf. on Robotics and Mechatronics, (ICROM), Tehran, Iran, 7-9 Oct. 2015.

[29] A. Olaru, "The optimizing space trajectory by using the inverse kinematics, direct dynamics and intelligent damper controlling with proper neural network, Int. Conf. on Advanced Mechatronic Systems, Tokyo, 2012.

[30] Olaru A., Masehian E., Olaru S., and Mihai N., Achieving extreme precisions for multiple manipulators using a proper coupled neural network matrix method and LabVIEW instrumentation, 4th Int. Conf. on Robotics and Mechatronics (ICROM), Tehran, 2016.

[31] Olaru A. and Olaru S., Assisted Optimisation of the Robot Dynamic Behavior with Magnetorheological Damper, 5th International Conference on MEMS NANO, and Smart Systems, Dubai, 2009